Hindawi Publishing Corporation
ISRN Astronomy and Astrophysics
Volume 2013, Article ID 170954, 8 pages
http://dx.doi.org/10.1155/2013/170954

Research Article

Phenomenological Description of Neutron Capture Cross Sections at 30 keV

M. Kiss[1] and Z. Trócsányi[2]

[1] *Berze N.J. Gimnázium, Kossuth 33, Gyöngyös 3200, Hungary*
[2] *Institute of Physics, University of Debrecen, P.O. Box 105, Debrecen 4010, Hungary*

Correspondence should be addressed to Z. Trócsányi; zoltan.trocsanyi@cern.ch

Received 7 December 2012; Accepted 26 December 2012

Academic Editors: H. Dehnen and R. Hawkes

Copyright © 2013 M. Kiss and Z. Trócsányi. This is an open access article distributed under the Creative Commons Attribution License, which permits unrestricted use, distribution, and reproduction in any medium, provided the original work is properly cited.

Studying the published values of Maxwellian-averaged neutron capture cross sections, we found simple phenomenological rules obeyed by the cross sections as a function of proton and neutron numbers. We use these rules to make predictions for cross sections of neutron capture on nuclei with proton number above 83, where very few MACS data are available. These predictions may be useful in certain models of nucleosynthesis of heavy nuclei in stars.

1. Introduction

Theoretical descriptions of nucleosynthesis in stars rely heavily on the knowledge of capture cross sections of slow neutrons on nuclei. The classical model of nucleosynthesis in weak neutron flux is based on slow neutron capture (the *s* process) that occurs along a path in the stability valley of nuclei (see, for instance, [1–4]). The *s*-process evolution codes take into account the most important processes (those with largest cross sections) along the stability valley. The necessary information on the neutron capture cross sections and β-decay life times, needed to describe qualitatively the abundances of the *s*-process elements, is rather well known from laboratory experiments [5–9].

The *s*-process model is capable to explain the observed abundance of heavy elements fairly well [10]. The difference of observation and prediction is largely attributed to another process that occurs in stellar environment with high neutron flux, typically in supernovae. In such circumstances, the neutron capture is very likely, and neutron-rich nuclei far from the stability valley build up very quickly due to repeated capture of neutrons. The nuclei produced in such a way are so unstable and short lived that experimental information about their capture cross sections and decay life times is not generally available.

In a recent work we proposed a unified model of nucleosynthesis of heavy elements in stars [11] that interpolates between the *s* process and *r* process smoothly. The approach takes into account all possible types of production and depletion mechanisms and solves the whole system of differential equations numerically. The result of such an approach is that (instead of the *s*-process path) the evolution of the synthesis proceeds along a band in the valley of stable nuclei. The width of this band—and consequently the final abundances of nuclei—depends on the neutron flux and the capture cross sections on individual nuclei characterized by both their proton and neutron numbers, $\sigma(Z, N)$, which constitute an essential input to the model calculations. Therefore, it is important to learn about these cross sections as much as possible.

In this paper, we study the general features of MACS collected in recent compilations [8, 9]. We used both measured and calculated cross sections. According to the Hauser-Feshbach (statistical) model, these cross sections can be computed, provided there are sufficiently many energy levels in the nucleus, which is usually satisfied by medium and heavy nuclei [12]. At 30 keV the calculated and measured cross sections agree within a factor of two [13], which is sufficient for our target precision. We have taken values of MACS from [14].

In Section 2 we show some phenomenological observations. In the following section we use those to make some order of magnitude predictions for the capture cross sections $\sigma(Z, N)$ for proton numbers $Z > 83$, where only very few MACS data are available. Section 4 contains our conclusions.

2. Observations

Neutron capture cross sections depend on the energy or equivalently the speed of neutrons. At moderate energies $\sigma \propto 1/v$ [10]; therefore, the averaged reaction rate $\langle \sigma v \rangle$ is approximately constant within a wide range of neutron energies (10–100 keV), relevant for nucleosynthesis of heavy elements in stars. As a result one can choose a convenient value for the temperature, traditionally $k_B T = 30$ keV.

There are cases when the capture cross section is due to several narrow resonances, or values at higher temperatures are necessary (for instance in the case of the astrophysical r process). Then one has to measure the cross section on a wider energy range (the range 1–300 keV is relevant for slow neutron capture) and compute the average with the Boltzmann energy distribution. In some measurement setup, it was possible to measure MACS directly [15]. These measurements showed that the neutron spectrum can be well approximated by a Maxwellian fit with temperature close to $k_B T = 30$ keV [3].

MACS at 30 keV have been calculated for many nuclei and made available in public depositories. Currently MACS values based on experimentally measured cross sections are available for stable and for some long-lived targets. For unstable ones cross sections obtained from theoretical reaction models are used for calculating MACS. A comprehensive and complete review of available MACS values has been presented recently in [9].

Studying the available MACS, we can make several observations: (i) although MACS of many nuclei are available, there are still many missing, or rather uncertain values, especially for nuclei with $Z > 83$ (see Figure 1 where all MACS, currently available, are shown); (ii) the cross sections vary over very large range of values (about four orders of magnitude); (iii) for any fixed neutron number N the cross section is maximal for a corresponding value of the proton number $Z_{\max}$ and decreases rapidly as $|Z - Z_{\max}|$ increases (see Figure 2). The last point implies that in the Z-N plain for each N there is a unique value $Z_{\max}(N)$ where the capture cross section attains its maximum value. The quantitative understanding of the existence of such a maximum is not our goal in the present paper.

If we plot the $Z_{\max}(N)$ function, a rather simple picture emerges: it appears that a simple, almost linear function can describe the MACS values, especially for small N. This feature becomes even more salient if we divide the nuclei into four groups according to the even/odd number of protons and neutrons: (i) $Z_{\max}^{(\mathrm{ee})}$ for Z even, N even, (ii) $Z_{\max}^{(\mathrm{oo})}$ for Z odd, N odd, (iii) $Z_{\max}^{(\mathrm{eo})}$ for Z even, N odd, and (iv) $Z_{\max}^{(\mathrm{oe})}$ for Z odd, N even, as shown in Figure 3.

In Figure 3 crosses mark the values of $Z_{\max}$ where the n-capture cross section is maximal for a fixed value of

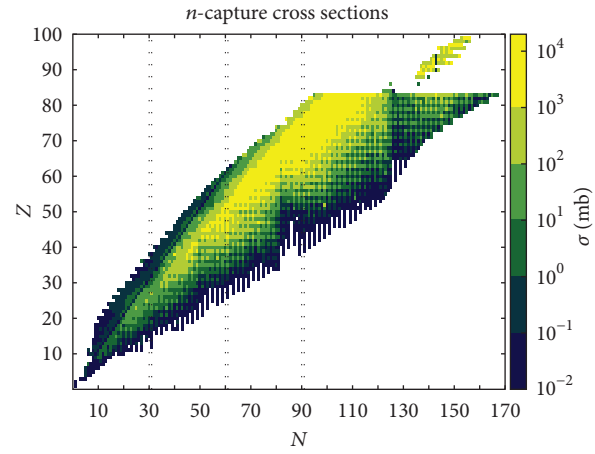

Figure 1: All presently available MACS (at 30 keV) on nuclei as a function of the proton and neutron numbers.

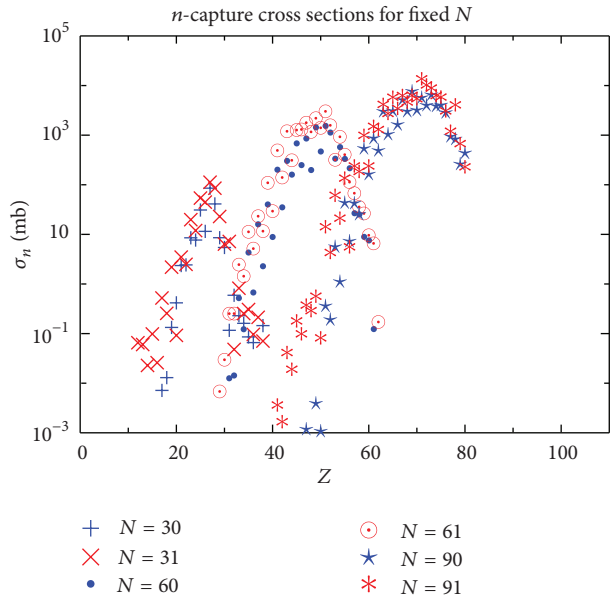

Figure 2: Dependence on the proton number Z of the MACS on nuclei with fixed neutron number $N = 30$, 31, 60, 61, 90, and 91 (indicated by vertical lines on Figure 1).

the neutron number N as taken from [8]. The solid lines represent fits of simple functions to these points in the form of

$$f(N; a_x, b, c) = \frac{N + a_x}{1 + bN^c}, \tag{1}$$

with a_x, b, and c being fitted parameters, and x = ee, oo, eo, or oe. We determined the values of these parameters in two steps. First, we minimized the function

$$\chi^2(a, b, c) = \sum_{i=1}^{214} \left(\frac{Z_{\max}(N_i) - f(N; a, b, c)}{\sigma_i} \right)^2, \tag{2}$$

that is, nuclei belonging to all four groups are taken into account. As the values of $Z_{\max}(N_i)$ can only be integers;

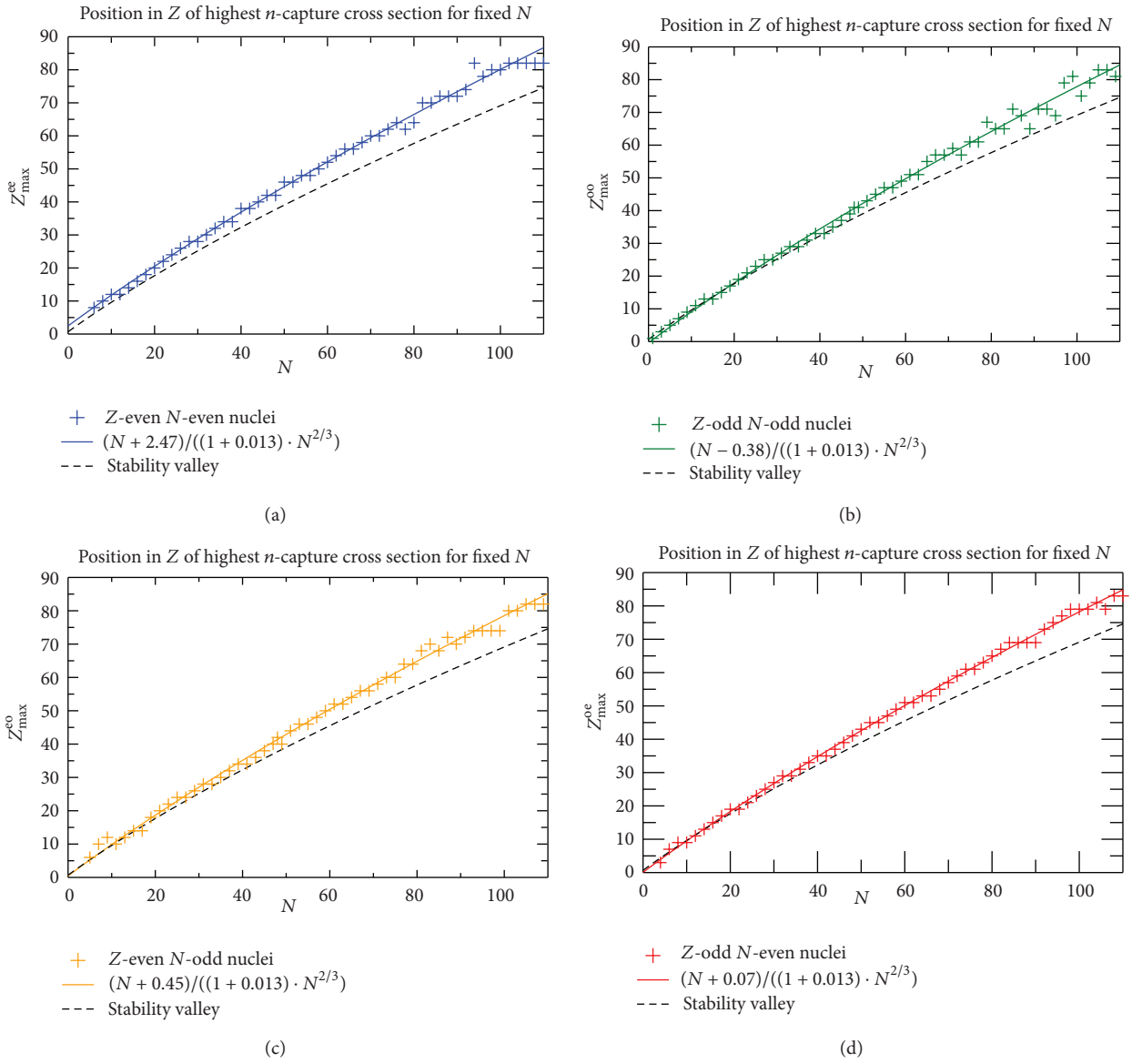

FIGURE 3: The function $Z_{max}(N)$ for even-even, odd-odd, even-odd, and odd-even nuclei. The crosses are the experimental values, and the solid line represents the fit to the function in (1). The dashed line runs through the bottom of the stability valley.

therefore, we assumed that the uncertainty of determining $Z_{max}(N_i)$ is $\sigma_i = 1$ for any i. The upper limit of the summation in each group was chosen as the largest value for which Z_{max} can be identified. With such a choice we find $N^{(x)}_{max} = 50$, 56, 53, and 55 maxima in the groups of even-even, odd-odd, even-odd, and odd-even nuclei, respectively, $(50 + 56 + 53 + 55 = 214)$. This fit gives

$$a = 0.60 \pm 0.08, \quad b = 0.013 \pm 0.0001, \quad c = 0.666 \pm 0.002, \tag{3}$$

with correlation index

$$i = \sqrt{1 - \frac{\chi^2(a,b,c)}{\sum_{i=1}^{214}\left(Z_{max}(N_i) - \overline{Z}\right)^2}} = \sqrt{1 - \frac{590.2}{116029}} = 0.997, \tag{4}$$

that is, the coefficient of determination is close to one, $i^2 = 0.994$ $(\overline{Z} = (1/214)\sum_{i=1}^{214} Z_{max}(N_i) = 45.5)$.

In the second step we minimize the functions

$$\chi^2(a_x) = \sum_{i=1}^{N^{(x)}_{max}}\left(\frac{Z^{(x)}_{max}(N_i) - f(N; a_x, 0.013, 0.666)}{\sigma_i}\right)^2 \tag{5}$$

separately for each group (x = ee, oo, eo, oe). (Again, we assume $\sigma_i = 1$ for all i). These fits give

$$a_{ee} = 2.47, \quad a_{oo} = -0.38, \quad a_{eo} = 0.45, \quad a_{oe} = 0.07, \tag{6}$$

with uncertainty being 0.16 and coefficient of determination above 0.99 in all cases. In principle the parameters b and c

could also depend on x, but such dependence did not show any improvement in the fits; therefore, we kept the fitted formula as universal as possible.

We also exhibit the line of the stability valley in Figure 3 as a function of N (instead of the usual $A = Z + N$)

$$Z_{\text{stab}} = \frac{N + a_s}{1 + b_s N^{c_s}}, \tag{7}$$

with parameters

$$a_s = 0.682, \quad b_s = 0.027, \quad c_s = 0.614. \tag{8}$$

We see clearly that the highest n-capture cross sections lie above the stability valley, and the separation grows with N.

We can also observe regularity in the Z dependence of the cross section at fixed N (see Figure 2). We can extrapolate this regularity as well as the $Z_{\max}$ values to the region in the nuclide chart where very few MACS values are available for n-capture cross sections on nuclei (nuclei with proton number above 83, see Figure 1).

The first observation is a simple trend in the behaviour of the function $\sigma_{\max}(N) \equiv \sigma(Z_{\max}(N))$. Putting $\sigma_{\max}(N)$ on a double logarithmic plot as shown in Figure 4(a) (left panel), we find that the general trend is well described by a fourth-order power function,

$$\sigma_{\max}(N) = \left(\frac{N}{10}\right)^4 \text{ mb}. \tag{9}$$

This general trend is slightly modulated with some oscillatory behaviour, with minima around magic numbers, as seen on Figure 4(b), where the ratios of the published cross sections [9] to $\sigma_{\max}(N)$ are shown.

The second observation is that if we normalize the cross sections $\sigma(Z, N)$ for a fixed neutron number N with the largest cross section $\sigma_{\max}(N)$, the profile of the dependence on the proton number is rather similar for all neutron numbers. This similarity is best seen if the position of the largest cross section is shifted by $-Z_{\max}$ to zero; therefore, we define these normalized and shifted cross section values by

$$\rho_N(z) = \frac{\sigma(z + Z_{\max}, N)}{\sigma_{\max}(N)} \equiv \frac{\sigma(Z, N)}{\sigma(Z_{\max}(N))}, \qquad z = Z - Z_{\max}, \tag{10}$$

for all values of N, where MACS values are available. Then we define the average z-dependence by

$$\rho(z) = \frac{1}{N_z} \sum_{N=1}^{N_z} \rho_N(z), \tag{11}$$

with squared standard deviation

$$\sigma(z)^2 = \frac{1}{N_z\,(N_z - 1)} \sum_{N=1}^{N_z} [\rho_N(z) - \rho(z)]^2, \tag{12}$$

where N_z is the number of available MACS values for fixed z. This average is shown in Figure 5. As seen from Figure 5(b) this function is well approximated with an almost exponential function in both positive and negative directions, but with different exponents. More precisely, we fit the logarithm of the average with quadratic functions of the form $\alpha_i z^2 + \beta_i z + \gamma_i$ with subscript of the coefficients referring to three regions in z: (i) $i = 1$ for $z < -26$, (ii) $i = 2$ for $-26 \le z < 0$, and (iii) $i = 3$ for $z > 0$. For $i = 2$ and 3 we fix $\gamma_i = 0$. This form ensures the constraint $\rho(0) = 1$. We also require the continuity of the fitted function at $z = -26$. We measure the goodness of the fit by the weighted sum of squares

$$\chi^2 \simeq \sum_z \frac{\left[\ln \rho(z) - \left(\alpha_i z^2 + \beta_i z + \gamma_i\right)\right]^2}{\left((\sigma(z))/\rho(z)\right)^2}, \tag{13}$$

summed over values of z in the three regions separately. The result of these fits is presented in Table 1 and shown in Figure 5.

Each function $\rho_N(z)$ differs from the average in two ways: (i) typically the larger N the wider $\rho_N(z)$ (as seen on Figure 1), (ii) in addition there are seemingly random fluctuations. The origin of the latter could be either a small physical effect or simply error of the measurement: there are published values for cross sections $\sigma(Z, N)$ that differ by a factor of two. While it is difficult to consider the effect of the latter, the first effect can be taken into account by a simple appropriate scaling of the width of the average to those of the functions $\rho_N(z)$, which we discuss in the next section.

3. Predictions

The phenomenological observations made in the previous section can be used to make predictions for the order of magnitude of neutron capture cross sections in regions of the nuclide chart where MACS values based on measured data are not available. We make these predictions in two steps. First we validate our procedure by comparing our predictions to published [9] cross sections. Then we use our procedure to make predictions.

3.1. Procedure. Our procedure relies on three pieces of information concluded from the analysis of the shape of *ridge of Maxwellian-averaged neutron capture cross sections*:

(1) position of $Z_{\max}$ as a function of the neutron number (location of the ridge top on the nuclide chart) obeys the simple function (1),

(2) values of $\sigma_{\max}(N)$ (height of the ridge for given value of $Z_{\max}(N)$) obey the simple function (9),

(3) characteristic behaviour of the average function $\rho(z)$ (slope of the ridge) is given by Figure 5.

In order to predict the cross section values for fixed neutron number, we proceed along the following steps.

(1) Given N, find the position of $Z_{\max}$ from (1), which gives two maxima, one for even proton numbers ($Z^{(\text{e})}_{\max}$) and one for odd proton numbers ($Z^{(\text{o})}_{\max}$).

(2) Given $Z_{\max}$ (either $Z^{(\text{e})}_{\max}$ or $Z^{(\text{o})}_{\max}$), position the maximum location of the average function $\rho(z)$ to $Z_{\max}$.

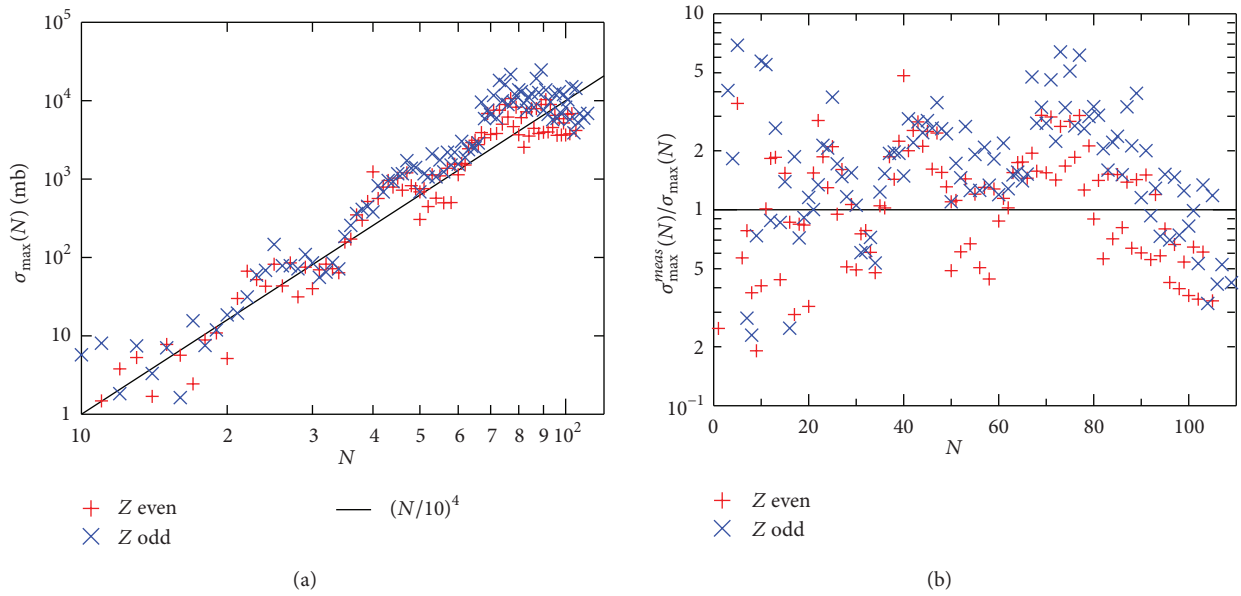

(a) (b)

FIGURE 4: (a) Largest neutron capture cross sections as a function of the neutron number. (b) Ratio of the published [9] largest cross sections to σ_{max} given in (9).

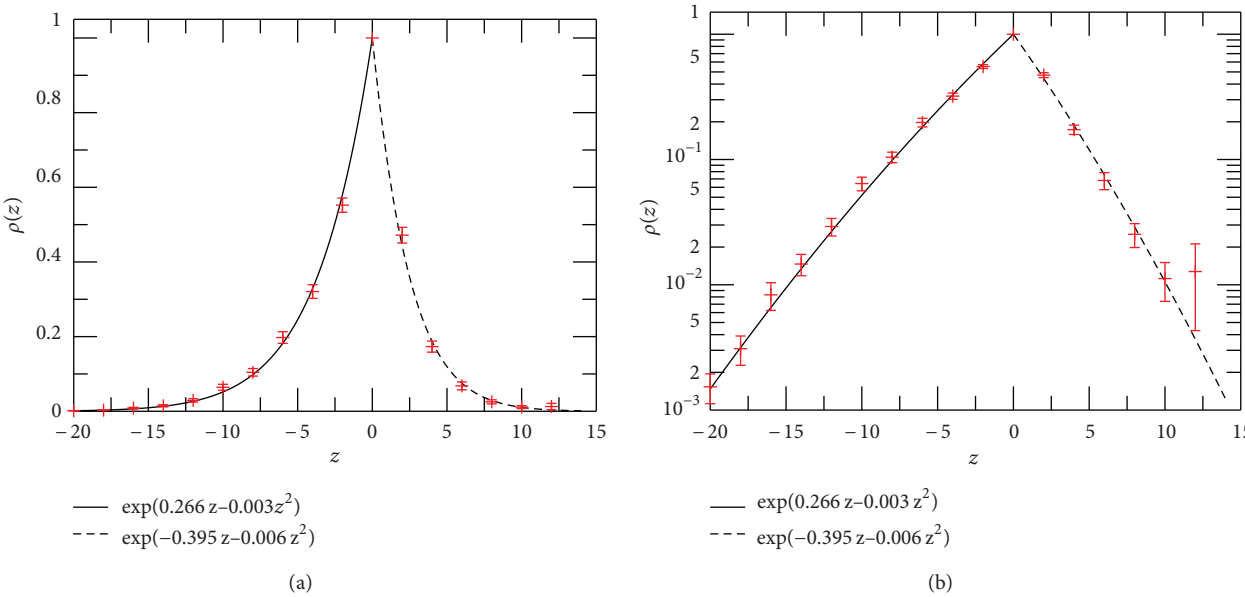

(a) (b)

FIGURE 5: Average of the normalized neutron capture cross sections as a function of $z = Z - Z_{max}$. The error bars represent the standard deviation $\sigma(z)$.

TABLE 1: Result of the fit to the average function $\rho(z)$.

i	α_i	β_i	γ_i	χ^2/d.o.f
1	0.0044	1.135	17.95	5.29/5
2	−0.0025	0.2658	0	6.15/9
3	−0.0058	−0.3948	0	7.14/4

Table 2: Ratios of largest and smallest published neutron capture cross sections ($R = \sigma_{max}/\sigma_{min}$) for nuclei beyond bismuth with $R > 5$ [9].

Nucleus	R	Nucleus	R	Nucleus	R
$^{227}_{89}Ac_{138}$	15.9	$^{231}_{90}Th_{141}$	16.7	$^{238}_{93}Np_{145}$	16.5
$^{246}_{94}Pu_{152}$	12.3	$^{242}_{95}Am_{147}$	22.7	$^{245}_{97}Bk_{148}$	12.4
$^{246}_{97}Bk_{149}$	6.41	$^{248}_{97}Bk_{151}$	7.13	$^{253}_{98}Cf_{155}$	20.0
$^{254}_{99}Es_{155}$	5.17	$^{251}_{99}Es_{152}$	7.48	$^{253}_{99}Es_{154}$	46.8

Table 3: Some predictions for neutron capture cross sections (in mb) as a function of the proton and neutron numbers for nuclei beyond bismuth. Based on the validation results, we estimate the relative uncertainty of the largest values along isotones below 10%.

Z	N															
	127	128	129	130	131	132	133	134	135	136	137	138	139	140	141	142
84	6	1	8	2	15	3	28	3	216	53	331	99	121	90	157	82
85	50	16	72	28	152	74	577	99	772	534	229	530	171	385	29	215
86	10	2	12	3	26	6	59	5	330	3	512	156	205	150	259	146
87	76	23	108	48	268	135	1024	163	1276	875	437	792	302	693	74	376
88	16	3	20	5	46	13	118	8	601	227	653	448	343	6	421	258
89	114	34	161	83	463	242	1786	266	2083	1560	2020	1366	523	1229	184	650
90	25	5	32	8	79	26	233	15	751	252	1400	429	1400	433	1550	484
91	171	49	237	139	786	428	3063	428	3359	2269	600	1770	695	2140	1213	2250
92	38	8	50	14	135	51	450	25	1118	412	1790	427	492	770	425	1550
93	253	70	346	229	1314	743	5168	681	5347	3590	2717	2514	1506	3692	600	1020
94	59	13	78	23	225	98	849	41	1648	666	2667	861	1496	1036	1693	750
95	370	100	500	374	2162	1267	8577	1069	8406	5613	4816	3635	2499	6256	2345	3093
96	90	20	120	37	371	184	1568	68	2407	1063	3938	1289	2383	1631	2635	2191
97	209	59	288	600	3500	2124	14000	1657	13048	8675	8379	5212	4087	10442	5132	5065
98	48	30	63	60	600	336	2831	111	3485	1675	5761	1913	3748	2538	4055	3611
99	115	34	162	295	1701	3500	6718	2536	20000	13250	14312	7411	6584	17168	10876	8185
100	25	16	32	30	291	600	5000	178	5000	2605	8353	2813	5820	3904	6172	5873

(3) Scale the height and width of the function $\rho(z)$ to the available MACS values by performing a two-parameter fit: (i) the scale factor of the height and (ii) the scale factor of the width.

The third step is hampered by the discrepancies in the published cross section values, which can sometimes be quite significant as shown in Table 2 for some heavy nuclei. Discrepancies exist among MACS values for lighter nuclei, but generally within a factor of two [9].

3.2. Validation. We can compare the values of the predicted cross sections to those calculated MACS [9] over the regions of the nuclide chart where values are abundantly available ($Z \leq 82$). In Figure 6 we show again the cross sections of Figure 2 together with the predicted values following from our procedure described in the previous subsection. Considering the simple nature of our procedure, the agreement is striking for all neutron numbers. Of course, the predictions rarely coincide exactly with the published values, but the order of magnitude is usually correct, especially where the cross sections are large, which is the most important region for nucleosynthesis. Similar agreement can be observed over the large region of the nuclide chart where published MACS are available.

3.3. Predictions of Unknown Cross Sections. Our procedure can be used to make prediction for cross sections in regions of the nuclide chart where *some* experimental information are available, such as $Z > 83$. In this region the general trend can be fitted to the published MACS to complete the ridge. With such a procedure we obtain cross section values shown in Table 3. We can now use those predictions to complete the picture exhibited on Figure 1. The result of such completion is shown in Figure 7.

4. Conclusions

We studied the dependence of the published MACS values on the proton and neutron numbers. We found a simple characteristic behaviour that we call the shape of the ridge of MACS in the nuclide chart. This shape can be described by the position and height of the ridge and the decrease of the slope. Although there are local deviations from this general trend, we were able to quantify these characteristics and made predictions for cross sections in regions of the nuclide chart where only few MACS values are available. Such predictions are needed for computer programs aimed at simulating the formation of all (i.e., not only along the *s*-process path) heavy nuclei in stars.

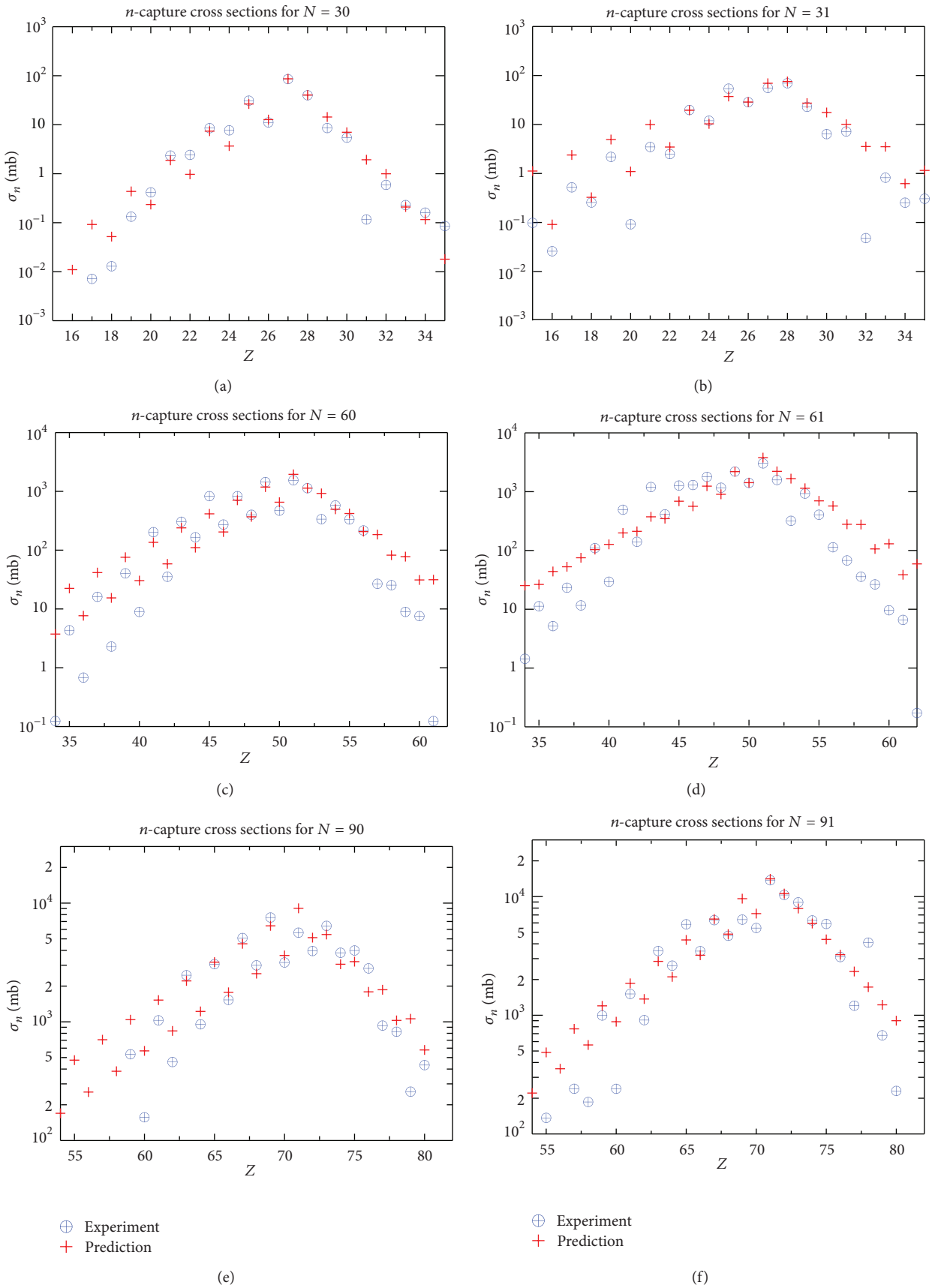

FIGURE 6: Dependence on the proton number Z of MACS (at 30 keV) on nuclei with fixed neutron number N = 30, 31, 60, 61, 90, and 91: comparison of the predictions of the phenomenological model to published MACS values.

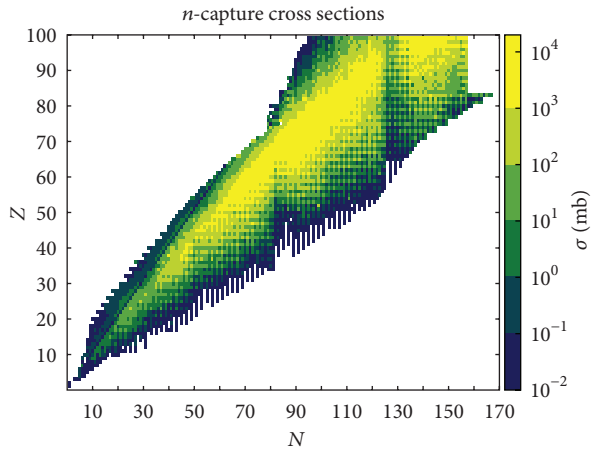

FIGURE 7: Ridge of MACS (at 30 KeV) on nuclei as a function of the proton and neutron numbers.

Acknowledgments

This paper was supported by the TÁMOP 4.2.1./B-09/1/KONV-2010-0007 Project. The authors are grateful to I. Angeli for the useful discussions.

References

[1] E. M. Burbidge, G. R. Burbidge, W. A. Fowler, and F. Hoyle, "Synthesis of the elements in stars," *Reviews of Modern Physics*, vol. 29, no. 4, pp. 547–650, 1957.

[2] A. G. W. Cameron, "Nuclear astrophysics," *Annual Review of Nuclear and Particle Science*, vol. 8, pp. 299–326, 1958.

[3] F. Käppeler, H. Beer, and K. Wisshak, "S-process nucleosynthesis-nuclear physics and the classical model," *Reports on Progress in Physics*, vol. 52, no. 8, article 945, 1989.

[4] R. Gallino, C. Arlandini, M. Busso et al., "Evolution and nucleosynthesis in low-mass asymptotic giant branch stars. II. Neutron capture and the s-process," *The Astrophysical Journal*, vol. 497, p. 388, 1998.

[5] T. Rauscher and F. K. Thielemann, "Astrophysical reaction rates from statistical model calculations," *Atomic Data and Nuclear Data Tables*, vol. 75, no. 1-2, p. 1, 2000.

[6] Z. Y. Bao, H. Beer, F. Käppeler, F. Voss, K. Wisshak, and T. Rauscher, "Neutron cross sections for nucleosynthesis studies," *Atomic Data and Nuclear Data Tables*, vol. 76, no. 1, pp. 70–154, 2000.

[7] I. Dillmann, M. Heil, F. Käppeler, R. Plag, T. Rauscher, and F. K. Thielemann, "KADoNiS—The Karlsruhe Astrophysical Database of Nucleosynthesis in Stars," *AIP Conference Proceedings*, vol. 819, pp. 123–127.

[8] T. Nakagawa, S. Chiba, T. Hayakawa, and T. Kajino, "Maxwellian-averaged neutron-induced reaction cross sections and astrophysical reaction rates for kT = 1 keV to 1 MeV calculated from microscopic neutron cross section library JENDL-3.3," *Atomic Data and Nuclear Data Tables*, vol. 91, no. 2, pp. 77–186, 2005.

[9] B. Pritychenko, S. F. Mughaghab, and A. A. Sonzogni, "Calculations of Maxwellian-averaged cross sections and astrophysical reaction rates using the ENDF/B-VII.0, JEFF-3.1, JENDL-3.3, and ENDF/B-VI.8 evaluated nuclear reaction data libraries," *Atomic Data and Nuclear Data Tables*, vol. 96, no. 6, pp. 645–748, 2010.

[10] C. E. Rolfs and W. S. Rodney, *Cauldrons in the Cosmos*, The University of Chicago Press, Chicago, Ill, USA, 1988.

[11] M. Kiss and Z. Trócsányi, "A unified model for nucleosynthesis of heavy elements in stars," *Journal of Physics*, vol. 4, Article ID 012024, 2010.

[12] K. Langanke, F. K. Thielemann, and M. Wiescher, "Nuclear astrophysicsand nuclei far from stability," *Lecture Notes in Physics*, vol. 651, Article ID 383467, pp. 383–467, 2004.

[13] F.-K. Thielemann, M. Arnould, and J. W. Truran, "Advances in nuclear astrophysics," in *Proceedings of the 2nd IAP Workshop*, Paris, France, July 1986.

[14] http://adg.llnl.gov/Research/RRSN/semr/30kev/rath00_7.4.30kev_calc.

[15] H. Beer and F. Käppeler, "Neutron capture cross sections on ^{138}Ba, ^{140,142}Ce, ^{175,176}Lu, and ^{181}Ta at 30 keV: prerequisite for investigation of the ^{176}Lu cosmic clock ," *Physical Review C*, vol. 21, no. 2, pp. 534–544, 1980.

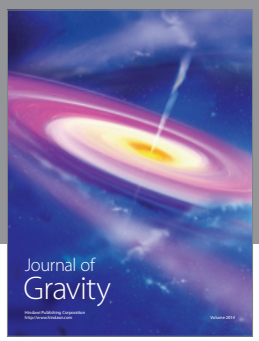

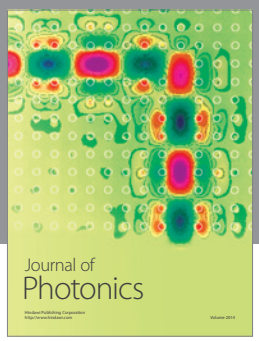

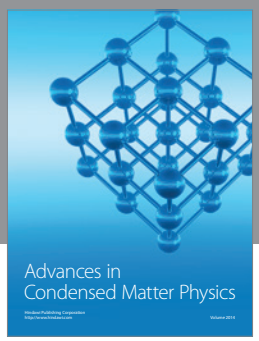

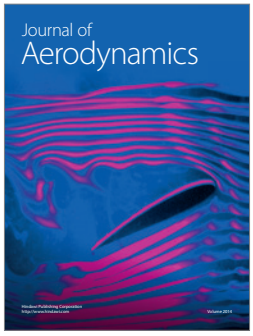

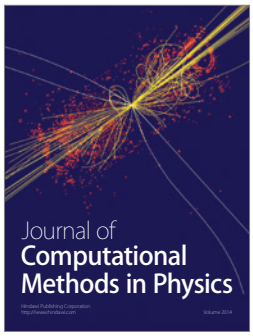

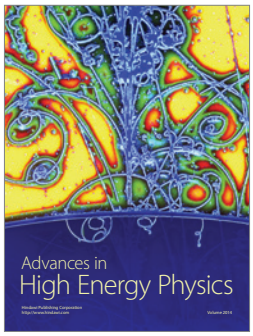

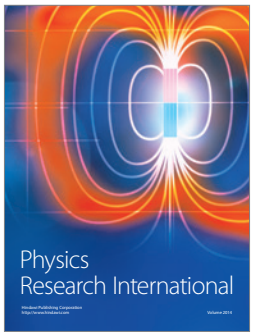

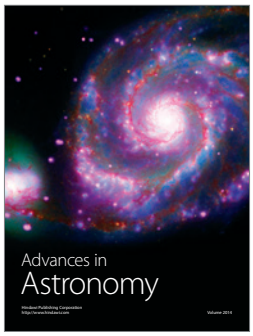

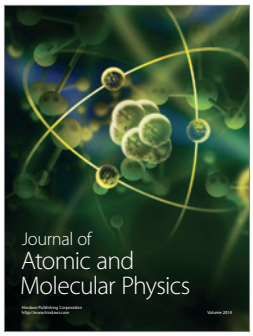

Hindawi

Submit your manuscripts at
http://www.hindawi.com